pH Dependent Formation of Unprecedented Water–Bromide Cluster in the Bromide Salts of PTP Assisted by Anion–π Interactions: Synthesis, Structure, and DFT Study

ARTICLE *in* JOURNAL OF CRYSTAL GROWTH · JANUARY 2014

Impact Factor: 1.7

CRYSTAL GROWTH & DESIGN

Article

pubs.acs.org/crystal

pH Dependent Formation of Unprecedented Water−Bromide Cluster in the Bromide Salts of PTP Assisted by Anion−π Interactions: Synthesis, Structure, and DFT Study

Prankrishna Manna,[†] Saikat Kumar Seth,[#] Antonio Bauzá,[⊥] Monojit Mitra,[†] Somnath Ray Choudhury,[†] Antonio Frontera,*[,⊥] and Subrata Mukhopadhyay*[,†]

[†]Department of Chemistry, Jadavpur University, Kolkata 700 032, India

[#]Department of Physics, M. G. Mahavidyalaya, Bhupatinagar, Purba Medinipur, West Bengal 721 425, India

[⊥]Departament de Química, Universitat de les Illes Balears, Crta. de Valldemossa km 7.5, 07122 Palma (Baleares), Spain

Supporting Information

ABSTRACT: Two new terpyridine derivatives $[PTPH_3](Br)_3 \cdot 3H_2O$ (**1**) and $[PTPH_3](Br_3)(Br)_2 \cdot H_2O$ (**2**), (PTP = 4′-(4-pyridyl)-2,2′:6′,2″-terpyridine) were synthesized and characterized by single crystal X-ray diffraction analyses. In **1**, intricate combination of anion···π/π−π/π···anion interactions generates the supramolecular network while **2** exhibits a combination of two different anion···π/π−π/π···anion and anion···π···anion assemblies. As anticipated, both of them are interlinked through hydrogen bonds affording molecular networks, but surprisingly, **1** shows hydrate aggregation and interactions with anions to generate water−bromide cluster blends in the solid lattices. A search of the crystal structure database (CSD) yielded only eight hits presenting an infinite tape in the solid state structure formed by bromide anions and water molecules, none of which had similar distribution of bromide and water as observed in **1**. Interestingly, in compound **1**, the bromide anion is involved in the formation of anion−water cluster and also engaged in anion···π interactions, thus generating a unique cluster of water−anion/anion···π/π−π/π···anion/anion−water cluster network. The different networks have been investigated by means of DFT calculations and the interactions characterized using the Bader's theory of "atoms-in-molecules".

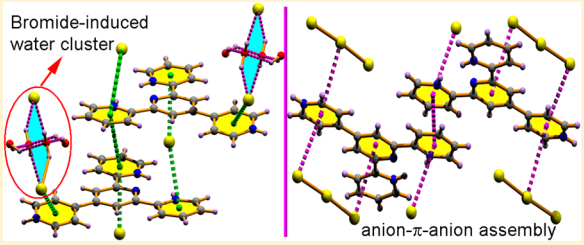

INTRODUCTION

Engineering supramolecular assembly is attracting continuous attention, mainly due to the innovative possibilities on how the structures were prepared with different size and shape[1] and how the assemblies are generated through a variety of cooperative noncovalent interactions. Though several noncovalent interactions such as hydrogen bonding,[2] π-stacking,[3] cation···π,[4] C−H···π,[5] and lone pair···π[6] forces govern the organization of multicomponent supramolecular assemblies, anion···π interactions[7] have added a new dimension in supramolecular assembly and have emerged as a new concept in anion-transport, anion-sensing, and anion-recognition chemistry[8] and transmembrane anion transport.[9] The importance of noncovalent anion···π interaction, which occurs between an electron-deficient aromatic system and a negatively charged species has been evidenced in gas phase,[10] solid state,[11] solution[12] and explored in detail by theoretical[13] as well as experimental[14] investigations.

Moreover, since crystal engineering is a difficult task to conceive due to the delicate nature of the noncovalent forces, the study of the impact of the acidity of reaction media leading to targeted species is still of transcendental importance. Triggering the synthetic procedures at different pH levels could lead to different degrees of protonation on the starting materials, for example, that we see here in this study and the supramolecular architecture may largely be diversified due to the presence of cooperative effects.[15] Herein, we examine detailed structural features of PTP complexes in revealing supramolecular extended networks generated through weak noncovalent forces. We also attempt to discern whether anion···π interactions are influenced by the pH value in building cooperative anion···π/π−π/π···anion and anion···π/π···anion type networks in the solid state. Furthermore, we seek to understand the role of hydrogen bonding, particularly involving the solvent water and anions in building unusual water−bromide clusters.

The cooperative behavior of water molecules leading to the formation of cluster networks is a prerequisite for unveiling the properties of water.[16] In the solid state, several water-clusters with different topologies have been reported in the context of crystal engineering.[17] The solvent water molecules not only bind themselves for the formation of clusters but also suitable anions take part in the assembly process to satisfy donor−acceptor balance and thus build water−anion clusters. However, only a few water−halide clusters[18] have been characterized in the solid state. This submission demonstrates

Received: October 29, 2013
Revised: December 17, 2013
Published: December 20, 2013

the pH dependence of lattice water aggregation with bromide anion by providing crystallographic evidence of a new form of water−bromide clusters.

We have studied the mutual influence of the hydrogen bonding interactions observed in the bromide−water cluster by means of DFT calculations. We have evaluated energetically how the presence of the bromide anions influence the strength of the hydrogen bonds observed in the water tetramer that is formed in the solid state. In addition, we have also analyzed synergistic effects between the different noncovalent interactions that participate in the formation of anion···π/π−π/π··· anion and anion···π/π···anion assemblies.

EXPERIMENTAL SECTION

Materials and Measurements. All reactions were carried out in aerobic condition and in aqueous medium. All chemicals used were of reagent grade and used as received. Freshly boiled, doubly distilled water was used throughout the synthetic procedure. IR spectra were recorded on a Perkin-Elmer RXI FT-IR spectrophotometer with the sample prepared as a KBr pellet, in the range of 4000−400 cm^{-1}. Elemental analyses (C, H, and N) were performed on a Perkin-Elmer 240C elemental analyzer. X-ray powder diffraction (XRPD) patterns of the samples were recorded on a Bruker D8 Advance instrument using Cu Kα radiation (λ = 1.5418 Å) (Figure S1 of the Supporting Information).

Synthesis. *Synthesis of $[PTPH_3](Br)_3{\cdot}3H_2O$ (1), (PTP = 4′-(4-pyridyl)-2,2′:6′,2″-terpyridine).* The PTP ligand was prepared following the literature method.[19] Aqueous suspension of PTP ligand (1.0 mM, 0.339 g) was dissolved at room temperature (~25.0 °C) by adding HBr with continuous stirring until pH reached in the range of 0.8−0.7 and then filtered to remove any undissolved materials. The yellow filtrate was kept for crystallization at room temperature (~25.0 °C). Block-shaped yellow single crystals of **1** were separated after several days from the mother liquor by slow evaporation at room temperature. The crystals were separated by filtration, washed with ice-cold water, and then air-dried. Anal. Calcd for $C_{20}H_{23}Br_3N_4O_3$ (**1**): C, 39.53; H, 3.82; N, 9.22%. Found: C, 39.52; H, 3.81; N, 9.21%. Main IR absorption bands observed for **1** (KBr pellet/cm^{-1}) are 3415 (w), 1833 (s), 1416 (vs), 1329 (s), 1290 (s), 1006 (s), 790 (w), 432 (s).

Synthesis of $[PTPH_3](Br_3)(Br)_2{\cdot}H_2O$ (2), (PTP = 4′-(4-pyridyl)-2,2′:6′,2″-terpyridine). Compound **2** was synthesized in the same way as described for **1**, except the pH which was adjusted to 0.5−0.4 by further addition of HBr. Block-shaped yellow single crystals of **2** were separated after several weeks (on more prolonged standing in comparison to that for **1**) from the mother liquor by slow evaporation at room temperature. The crystals were separated by filtration, washed with ice-cold water, and then air-dried. Anal. Calcd for $C_{20}H_{19}Br_5N_4O$ (**2**): C, 32.83; H, 2.62; N, 7.66%. Found: C, 32.82; H, 2.61; N, 7.65%. Main IR absorption bands observed for **2** (KBr pellet/cm^{-1}) are 3416 (w), 1834 (s), 1416 (vs), 1383 (s), 1290 (s), 1006 (s), 950 (w), 499 (s).

X-ray Crystallographic Analysis. Single crystal X-ray diffraction intensity data of both **1** and **2** were collected at 150(2) K using a Bruker APEX-II CCD diffractometer equipped with graphite monochromated Mo Kα radiation (λ = 0.71073 Å). Data reduction was carried out using the program Bruker SAINT.[20] An empirical absorption correction SADABS[21] was applied. The structure of the title complexes were solved by direct method and refined by the full-matrix least-squares technique on F^2 with anisotropic thermal parameters to describe the thermal motions of all nonhydrogen atoms using the programs SHELXS97 and SHELXL97,[22] respectively. All calculations were carried out using PLATON[23] and WinGX system Ver-1.64.[24] All hydrogen atoms were located from difference Fourier map and refined isotropically. A summary of crystal data and relevant refinement parameters are given in Table S1 of the Supporting Information.

Theoretical Methods. The energies of all the species included in this study were computed at the BP86-D3/def2-TZVPD level of theory using the crystallographic coordinates within the program TURBOMOLE, version 6.4.[25] The interaction energies were calculated with correction for the basis set superposition error (BSSE) by using the Boys−Bernardi counterpoise technique.[26] For the calculations, we have used the BP86 functional with the latest available correction for dispersion (D3). The "atoms-in-molecules" (AIM)[27] analysis was performed at the BP86/def2-TZVP level of theory. The calculation of AIM properties was done using the AIMAll program.[28]

RESULTS AND DISCUSSION

XRPD Studies. Only a small change in the acidity of the reaction media appears to be responsible for the formation of different products **1** or **2**. It could be noted here that as the preparation of compound **2** needs more prolonged standing of the reaction mixture in a bromide-rich medium, a partial oxidation process might occur and that is reflected in the anionic charge distribution in **2** where three negative charges are distributed over five bromide atoms (Br_3^- and $2Br^-$) whereas over three bromide atoms ($3Br^-$) in **1** (suggestion of a reviewer). Exclusive generation of **1** and **2** under the specific reaction media within a narrow pH window was checked by XRPD experiments several times when a detectable difference in the XRPD patterns (Figure S1 of the Supporting Information) between **1** and **2** was observed. We like to mention here that due to the solubility problem, we were unable to synthesize any other differently protonated PTP species at higher pH.

Crystallographic Analysis. The asymmetric units of both **1** and **2** consists of one triply protonated PTP molecule, three solvent water molecules, and three bromide anions for **1**, whereas **2** consists of one solvent water molecule, one Br_3^-, and two Br^-. Figure 1 represents the diagram of the parent triply protonated PTP molecule with a common atom numbering scheme. In both the complexes, among four pyridine N atoms, outer three N atoms (N1, N3, and N4) get protonated under the reaction conditions. The adjacent pyridine nitrogen atoms of the rings 1A, 2, and 1B form an isosceles triangle (Figure 1). The halide ions are in contact to the triply protonated $PTPH_3$ cationic species through $(N-H)^+\cdots Br^-$ ionic hydrogen bond[29] and $CH^{\delta+}\cdots Br^-$ interactions.[30]

In the solid state structure of **1**, one of the counterions (Br2) binds to the protonated pyridine ring nitrogen atoms N1 and N3 of ring 1A and 1B through N1−H1···Br2 and N3−H3···Br2 hydrogen bonds (Table 1) and generates a $R_2^1(10)$ ring motif, which may be denoted as $D_1^1(2)D_1^1(2)R_2^1(10)$, according to the graph-set notation.[31] On either side of the parent $PTPH_3$ species, another bromide ion Br3 is in contact with the pyridine ring carbon atoms C12 and C20 of ring 1B and ring 3, respectively, to generate another $R_2^1(10)$ ring motif (Figure S2 of the Supporting Information). The remaining anion Br1 atom is in contact through the pyridine ring carbon atoms C4, C15,

dx.doi.org/10.1021/cg401615r | Cryst. Growth Des. 2014, 14, 747−755

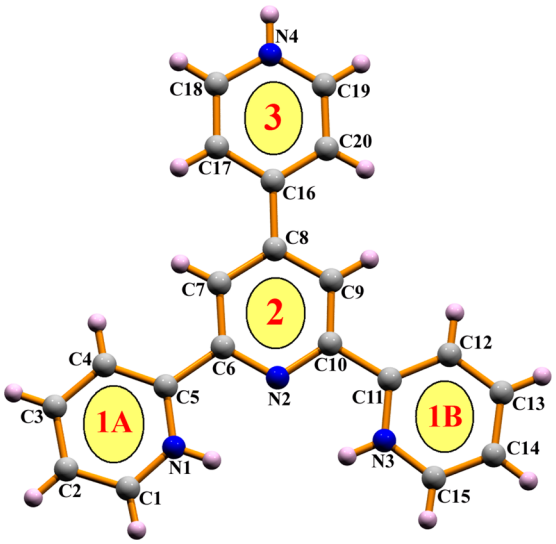

Figure 1. Representation of the $PTPH_3$ molecule with the common atom numbering scheme used in complexes **1** and **2**. Rings 1A, 1B, and 3 are positively charged due to the protonation.

and C17 of protonated pyridine rings 1A, 1B, and 3, respectively. Moreover, the solvent water molecules also interact with the anionic species. Therefore, the binding of bromide anions and water molecules by the $PTPH_3$ molecule is responsible for the solid state assembly of $PTPH_3$:(3Br, $3H_2O$) complex.

The anion Br3 is accommodated through C12−H12···Br3 and C20−H20···Br3 hydrogen bonds at one of the side basins of $PTPH_3$ molecules. This Br3 atom acts as an acceptor to the solvent water oxygen O2 in the molecule at (x, y, z) and $(-x, -y + 2, -z)$. This solvent water oxygen atom acts as a double hydrogen bond donor to the anionic Br3 (Table 1). Thus, a centrosymmetric dimeric ring $R_4^2(8)$ ring (A) centered at (0 1 0) (Figure S2 of the Supporting Information) is generated and can be represented using graph set notation[31] as $D_1^1(2)$ $D_1^1(2)$ $D_1^1(2)$ $D_1^1(2)$ $[R_4^2(8)]$. Interestingly, the neighboring water oxygen atom O3 acts as double donor to the water oxygen atom O2 in the molecule at (x, y, z) and $(-x + 1, -y + 2, -z)$. Thus again a centrosymmetric ring $D_1^1(2)$ $D_1^1(2)$ $D_1^1(2)$ $D_1^1(2)$ $[R_4^2(8)]$ (B) was formed which is centered at (1/2, 1, and 0) (Figure S2 of the Supporting Information). Again, the solvent water oxygen O2 acts as double donor to Br3 and thus solvent water and bromide anions arrange themselves to propagate ABAB····· chains along the (1 0 0) direction (Figure S2 of the Supporting Information). Thus a unique water tetramer and water−bromide tape is generated through hydrogen-bonding interactions, where the core of this tape is constituted by planar water tetramers and water−bromide dimers and propagates through successive tetramers and dimers (Figure S2 of the Supporting Information). The pyridine ring carbon C3 in the molecule at (x, y, z) acts as donor to the water oxygen atom O3 in the molecule at $(-x, y - 1/2, -z + 1/2)$, connecting the $PTPH_3$ moieties to the unique water and water−bromide tape. Moreover, on either side of the $PTPH_3$, C12, C20 atoms bind the water−bromide dimer and C3 atom binds water tetramer successively. Consequently, a 2D supramolecular network is formed in the (1 1 0) plane where successive water and water−bromide tape is the main building block in **1** (Figure S2 of the Supporting Information).

In another structural motif of **1**, C4 and C17 atoms of ring 1A and ring 3 in the molecule at (x, y, z) acts as donor to the halide Br1 atom at $(-x, y + 1/2, -z + 1/2)$, generating $D_1^1(2)D_1^1(2)[R_2^1(10)]$ motif such that Br1 is accommodated in one side of $PTPH_3$ species (Figure S3 of the Supporting Information). Again, halide Br2 is accommodated to one side of $PTPH_3$ through N−H···Br hydrogen bonds forming another $D_1^1(2)D_1^1(2)[R_2^1(10)]$ ring motif. Also, 1A ring carbon atom C15 acts as donor to Br1 at $(-x, y + 1/2, -z + 1/2)$, and the neighboring solvent water oxygen O1 acts as double donor to the Br1 and Br2 (Table 1). Thus a $R_4^2(9)$ ring motif is formed in **1** (Figure S3 of the Supporting Information) and again this Br1 acts as acceptor to the carbon atoms C4 of ring 1A and C17 of ring 3, generating a 1D ribbon propagating along the (1 0 0) direction. Interestingly, among the parallel tapes, the pyridine ring nitrogen N4 atom is juxtaposed to the solvent water oxygen O1 in the molecule at (x, y, z) and $(x - 1, y + 1, z)$, thus generating the $R_6^4(16)$ ring motif and a 2D supramolecular network is propagating in the (1 1 0) plane (Figure S3 of the Supporting Information), whose formation is

Table 1. Hydrogen Bonding Geometry of $C_{20}H_{23}Br_3N_4O_3$ (1) (Å, deg)

D−H···A	*d*(D−H)	*d*(H···A)	*d*(D···A)	D−H···A	symmetry
N(1)−H(1)···N(2)	0.86	2.28	2.665(7)	107	−
N(3)−H(3)···N(2)	0.86	2.29	2.669(7)	107	−
N(1)−H(1)···Br(2)	0.86	2.45	3.213(5)	148	−
N(3)−H(3)···Br(2)	0.86	2.44	3.202(5)	148	−
O(1)−H(1O1)···Br(2)	0.83	2.47	3.289(5)	168	$-x + 1, y - 1/2, -z + 1/2$
O(1)−H(2O1)···Br(1)	0.81	2.53	3.277(5)	155	$x, -y + 1/2, z + 1/2$
O(2)−H(1O2)···Br(3)	0.93	2.42	3.292(5)	157	−
O(2)−H(2O2)···Br(3)	0.82	2.52	3.326(6)	168	$-x, -y + 2, -z$
N(4)−H(4)···O(1)	0.86	1.82	2.649(7)	160	$x - 1, y + 1, z$
O(3)−H(1O3)···O(2)	0.87	2.13	2.860(10)	141	−
O(3)−H(2O3)···O(2)	0.86	2.06	2.852(9)	153	$-x + 1, -y + 2, -z$
C(3)−H(3A)···O(3)	0.93	2.59	3.227(10)	126	$-x, y - 1/2, -z + 1/2$
C(4)−H(4A)···Br(1)	0.93	2.73	3.649(6)	171	$-x, y + 1/2, -z + 1/2$
C(12)−H(12)···Br(3)	0.93	2.81	3.699(6)	160	−
C(15)−H(15)···Br(1)	0.93	2.87	3.532(6)	129	$-x + 1, -y + 1, -z$
C(17)−H(17)···Br(1)	0.93	2.73	3.613(7)	158	$-x, y + 1/2, -z + 1/2$
C(20)−H(20)···Br(3)	0.93	2.86	3.685(7)	150	−

dx.doi.org/10.1021/cg401615r | *Cryst. Growth Des.* 2014, 14, 747−755

readily analyzed in terms of small building blocks with finite zero-dimensional ring motifs.

Due to the presence of anionic bromide atoms, the $PTPH_3$ cation interacts strongly among themselves through multi π-stacking interactions. Moreover, the solid state structure possesses a remarkable supramolecular architecture through novel anion···π interaction.[32] One anion Br1 is oriented toward the π-cloud of pyridinium ring 1A (Figure 2). The separation

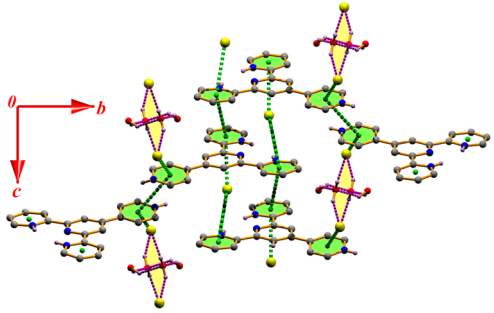

Figure 2. Cooperativity of anion···$\pi/\pi-\pi/\pi$···anion and anion−water cluster in **1**.

distance between the ring centroid and the Br1 anion is 3.645(2)Å. The shortest separation distance reflecting this interaction is Br1···N1 = 3.325 Å, which is below the sum of the corresponding van der Waals radii[33] and suggesting significant anion···π interaction. Again the centroid of the pyridine ring 1A is involved in face-to-face $\pi-\pi$ stacking interaction with another pyridine ring 1B. The ring 1A of the molecules at (x, y, z) is in contact with ring 1B of the partner molecule at $(x, 3/2 - y, 1/2 + z)$ with a ring centroid separation of 3.571(4)Å. The halide Br1 ion is again approaching the centroid of the pyridine ring 1B with a separation of 3.639 Å (Figure 2), suggesting anion···π interaction.[32] The shortest separation distance reflecting this interaction is Br1···C11 = 3.321 Å, which is below the sum of the corresponding van der Waals radii.[33] Therefore, the self-assembly involves very rare cooperative anion···$\pi/\pi-\pi/\pi$··· anion network in **1**.

The anion Br3 is oriented toward the π-face of the pyridine ring 3, where the distance between the ring centroid and Br3 is 4.23 Å. The shortest separation distance between Br3 and C18 is 3.529 Å, suggesting weak anion···π interaction in **1**. Interestingly, the molecular packing of $PTPH_3$ species is such that the $\pi-\pi$ stacking between the pyridine ring 3 of adjacent moiety is optimized. The pyridinium ring 3 of the $PTPH_3$ at (x, y, z) and $(-x, 2 - y, 1 - z)$ are strictly parallel, with an interplanar spacing of 3.563(3)Å and an intercentroid separation of 4.199(5)Å, corresponding to a ring offset of 2.222 Å. Again this pyridine ring 3 is in contact with the Br3 anion through significant anion···π interaction (Figure 2). Thus the entire assembly produces an associative multi anion···$\pi/\pi-\pi/\pi$···anion network and these noncovalent forces recognize themselves in a cooperative manner, which results in a supramolecular unique layer framework in **1** (Figure 3). Since the anion Br3 is responsible for the formation of water−bromide cluster and is involved in anion···π interaction with the π-cloud of ring 3, we may designate the supramolecular association as a water···anion/anion···$\pi/\pi-\pi/\pi$···anion/anion··· water network (Figure 3). This entire assembly produces a new supramolecular network and illustrates the occurrence of an elegant combination of noncovalent forces in the solid state structure of **1**.

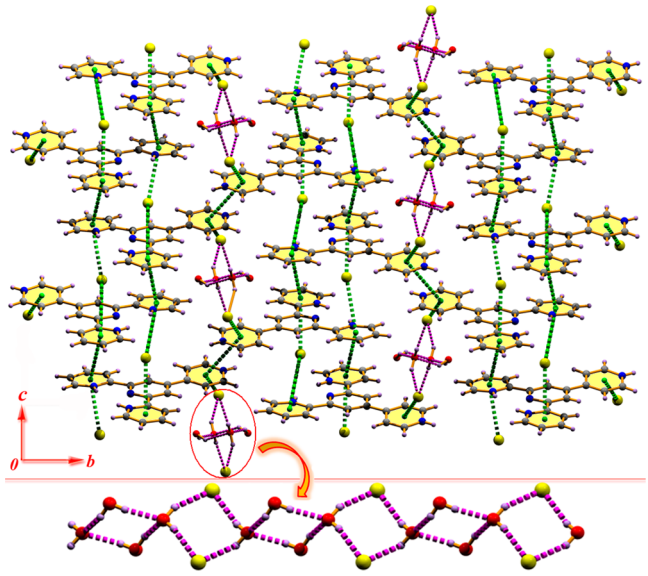

Figure 3. Perspective view of supramo lecular assembly through anion···$\pi/\pi-\pi/\pi$···anion and water···anion/anion···$\pi/\pi-\pi/\pi$···anion/anion···water associative network. Inset: water tetramer and water bromide tape in **1**.

Compound **2** includes a combination of various hydrogen bonds, $\pi-\pi$ stacking, and anion−π interactions in the solid state (Table 2). In one side of the $PTPH_3$ cation, one anion Br1 is entrapped through the protonated pyridine ring nitrogen atoms N1 and N3 by strong N−H···Br bonds (Table 2) to generate the $D_1^1(2)$ $D_1^1(2)$ $R_2^1(10)$ motif (Figure S4 of the Supporting Information). The rest protonated pyridine ring nitrogen N4 is in contact with the Br2 atom on the opposite side. Interestingly, the pyridine ring carbon C19 in the molecule at (x, y, z) interacts with the Br2 atom in the molecule at $(-x + 1, -y + 2, -z + 1)$ to extend the network. Two Br2 atoms again interact with the pyridine nitrogen N4 and pyridine ring carbon C19 of the partner molecule just due to their self-complementarities and thus generates a $R_4^2(10)$ dimeric ring motif in **2** (Figure S4 of the Supporting Information). On either side of the building block, $PTPH_3$ also binds Br_3^- anions and the solvent water molecule to extend the network. The pyridine ring carbon atoms C4 and C18 interact with the Br3 and Br4 atoms respectively to generate the $R_2^2(12)$ motif. The carbon atom C3 of pyridine ring 1A also interacts with the Br3 atom (Table 3) of the neighbor molecule at $(-x, -y, -z + 1)$, which is also interacting with the C4 atom of partner 1A ring of $PTPH_3$, so another $R_4^2(10)$ dimeric ring motif is generated. On another side, the carbon atoms C9, C12, and C20 of ring 1B, 2, and 3, respectively, interact with the solvent water O1 in the molecule at $(-x + 1, -y + 2, -z + 1)$ and creates two $R_2^1(7)$ ring motifs (Figure S4 of the Supporting Information). This solvent water molecule O1 also interacts with the Br2 atom and the repetition of these small building blocks (i.e., ring motifs creates a 2D supramolecular network in **2** (Figure S4 of the Supporting Information).

Another interesting feature of the structure is that the Br3 atom of the Br_3^- moiety is oriented toward the centroid of the pyridinium ring 3 in the molecule at $(-x, 1 - y, 1 - z)$ and again juxtaposed by the Br4 atom through the anion···π interaction (Figure 4). The separation distance between the ring centroid and the anions Br3 and Br4 are 3.612(4)Å and 3.821(3)Å, respectively. The shortest separation distances are

dx.doi.org/10.1021/cg401615r | Cryst. Growth Des. 2014, 14, 747−755

Table 2. Hydrogen Bonding Geometry of $C_{20}H_{19}Br_5N_4O$ (2) (Å, deg)

D−H···A	d(D−H)	d(H···A)	d(D···A)	D−H···A	symmetry
N(1)−H(1A)···N(2)	0.86	2.31	2.679(9)	106	−
N(3)−H(3)···N(2)	0.86	2.22	2.623(9)	108	−
N(1)−H(1A)···Br(1)	0.86	2.45	3.213(6)	148	−
N(3)−H(3)···Br(1)	0.86	2.50	3.243(6)	145	−
N(4)−H(4)···Br(2)	0.86	2.38	3.223(6)	166	−
O(1)−H(1O1)···Br(2)	0.86	2.48	3.290(6)	158	−
O(1)−H(2O1)···Br(1)	0.86	2.73	3.473(6)	145	$x, y + 1, z + 1$
C(9)−H(9)···O(1)	0.93	2.54	3.462(9)	172	$-x + 1, -y + 2, -z + 1$
C(12)−H(12)···O(1)	0.93	2.34	3.261(10)	169	$-x + 1, -y + 2, -z + 1$
C(20)−H(20)···O(1)	0.93	2.58	3.493(9)	167	$-x + 1, -y + 2, -z + 1$
C(3)−H(3A)···Br(3)	0.93	2.90	3.822(8)	170	$-x, -y, -z + 1$
C(4)−H(4A)···Br(3)	0.93	2.73	3.590(8)	154	−
C(15)−H(15)···Br(5)	0.93	2.62	3.442(8)	148	$x, y, z - 1$
C(18)−H(18)···Br(4)	0.93	2.87	3.588(8)	135	−
C(19)−H(19)···Br(2)	0.93	2.79	3.606(8)	148	$-x + 1, -y + 2, -z + 1$

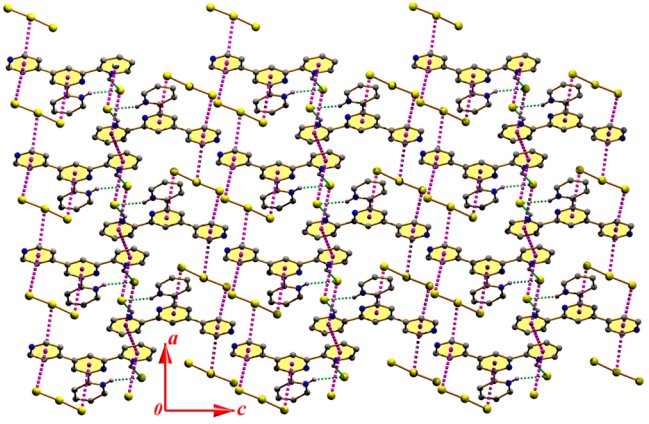

Figure 4. Supramolecular assembly in **2**, generated through associative anion···π/π···anion and anion···$\pi/\pi-\pi/\pi$···anion interactions.

Br3···C18 = 3.518(2)Å and Br4···C19 = 3.433(2)Å, which are below the sum of the corresponding van der Waals radii[33] and suggesting significant anion···π interaction which leads to an unique anion···π/π···anion type supramolecular framework in **2** (Figure 4). Again, Br5 atom of Br_3^- anion is in contact to the unprotonated pyridine ring 2 with a separation distance of 3.824(3)Å, where the shortest separation distance is Br5···C6 = 3.474(2)Å. Surprisingly, anion Br1 is oriented toward the π-cloud of protonated pyridine ring 1B with a separation of 3.760(2)Å to the ring centroid. The shortest separation distance Br1···C11 = 3.603(2)Å is below the sum of the corresponding van der Waals radii, suggesting significant anion···π interaction. The molecular packing is such that the $\pi-\pi$ stacking interactions between the adjacent $PTPH_3$ molecules are optimized. The pyridine ring 1B of the molecules at (x, y, z) and $(1 - x, 1 - y, -z)$ are strictly parallel, with an interplanar spacing of 3.425 Å, and a ring centroid separation 3.750(5)Å, corresponding to the ring offset of 1.529 Å. This pyridine ring 1B is again in contact with Br1 atom through anion−π interaction (Figure 4). Thus, this entire assembly displays a very rare supramolecular anion···$\pi/\pi-\pi/\pi$···anion network and produces the occurrence of a graceful blend of weak forces in the solid state. The intact supramolecular layer scaffold (Figure 4) has been unraveled where anion···π/π···anion and anion···$\pi/\pi-\pi/\pi$···anion cooperative types of weak noncovalent forces act in a unison accommodating mode.

Theoretical Study. We have focused our theoretical study to analyze the energetic features of the interesting supramolecular assemblies described above. As previously mentioned, the protonated $PTPH_3$ cation acts as a host for the bromide counterions due to its enhanced capabilities of establishing hydrogen bond, $\pi-\pi$, and anion−π interactions. Our study was focused on the different binding modes of the $PTPH_3$ receptor, which clearly influence the final solid state architecture of both crystal structures. On the one hand, compound **1** $[PTPH_3](Br)_3{\cdot}3H_2O$ is formed by a combination of $PTPH_3$ and bromides acting as counterions. As described, the $PTPH_3$−bromide complexes are stacked along infinite chains establishing anion−π, $\pi-\pi$ stacking, and hydrogen-bonding interactions. Particularly, one interesting feature of compound **1** is the presence of water−bromide clusters, which significantly stabilize the structure. In compound **2**, additionally to Br^-, Br_3^- is also present as a counterion, leading to the establishment of different anion−π interactions, with one or two Br atoms placed over the $PTPH_3$ cation. We have treated the $PTPH_3$ π-system together with three counterions, as a unique entity for the calculations in order to evaluate the $\pi-\pi$ and anion−π interactions using a neutral model.

As aforementioned, in compound **1** the supramolecular assembly is formed by the combination of anion−$\pi/\pi-\pi/\pi$−anion interactions. The theoretical model used to evaluate the interactions is shown in Figure 5. We have evaluated the binding energy associated to the different noncovalent

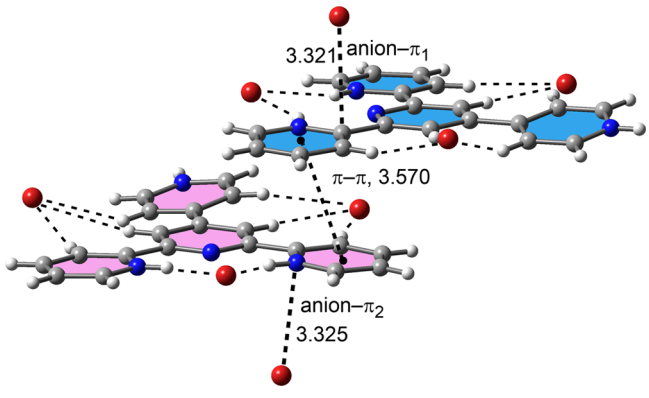

Figure 5. Theoretical model used to evaluate the anion−$\pi/\pi-\pi/\pi$−anion assembly of compound **1**. Distances are in Ångströms.

dx.doi.org/10.1021/cg401615r | Cryst. Growth Des. 2014, 14, 747−755

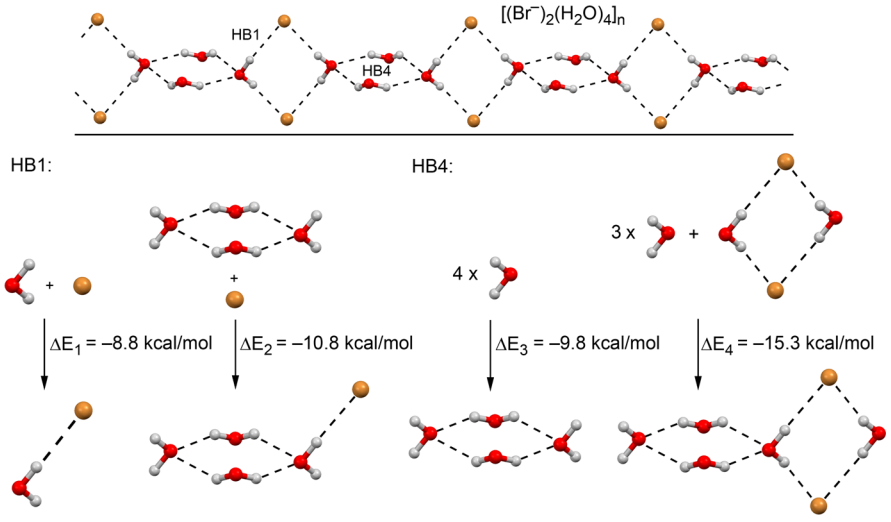

Figure 6. Top: water–bromide cluster present in compound **1**. Bottom: Equations used to evaluate cooperativity effects.

interactions. First, the anion–π_1 interaction, which is basically established between bromide and one carbon atom of the protonated pyridine moiety, contributes to −24.0 kcal/mol. In spite of the fact that we are using a neutral model, this considerably strong interaction is due to the protonated state of pyridine, resulting in a considerable strengthening of the interaction.[34] The anion–π distance (3.32 Å) is comparable to common values observed for anion–π complexes involving bromide. Surprisingly, the binding energy of the π–π stacking interaction is very high, (i.e., −26.0 kcal/mol). This is due to secondary interactions between the bromide ions of one layer with the $PTPH_3$ cations of the other layer and vice versa. Finally, the anion–π_2 that is established between the Br^- and the nitrogen atom of the organic ligand interaction resulted in a −29.8 kcal/mol energy value. As in the case of the anion–π_1, the protonation state of the $PTPH_3$ molecule in the solid state strengthens the interaction due to the presence of an explicit positive charge in the pyridine ring.

In addition, we have studied the mutual influence of the hydrogen-bonding interactions observed in the bromide–water cluster of **1**. We have evaluated how the presence of the bromide anions influence the strength of the hydrogen bonds established between the water molecules to form the water tetramer and vice versa. To achieve this we have used the equations shown in Figure 6. We have evaluated the interaction energy of a single $Br^-\cdots H_2O$ hydrogen bond (HB1 in Figure 6) using the X-ray geometry, denoted as ΔE_1. Moreover, we have evaluated this interaction energy, considering that the water tetramer has been previously formed (ΔE_2). As a result, the ΔE_2 energy is 2 kcal/mol more favorable than ΔE_1, suggesting that the presence of the water tetramer reinforces the $Br^-\cdots H_2O$ hydrogen bond. In order to evaluate the influence of the $Br^-\cdots H_2O$ hydrogen bonds on the formation energy of the tetramer (HB4, see Figure 6), we have computed the formation energy without (ΔE_3) and with (ΔE_4) the presence of the bromide ions. The energies are included in Figure 6, and it can be observed that the formation energy of the water tetramer is ΔE_3 = −9.8 kcal/mol and the formation energy of the tetramer considering that one water molecule is already interacting with two bromide ions is ΔE_4 = −15.3 kcal/mol, indicating a strong influence on the interaction energy. This energetic analysis clearly indicates the mutual influence of both interactions ($Br^-\cdots H_2O$ and $H_2O\cdots H_2O$) that leads to favorable cooperativity effects.

We have also examined the Cambridge Structural Database,[35] which is a big depot of geometrical information, to learn whether the water–bromide cluster observed in compound **1** is common in X-ray structures. We have found eight compounds presenting an infinite tape in the solid state structure formed by bromide anions and water molecules. None of them presents the same distribution of bromide and water molecules observed in **1**. In Scheme 1, we have represented the three different distributions of anion–water associative networks found in the CSD and their reference codes. We have also included the network observed in compound **1** for comparison purposes. The most common distribution is the one formed by fused hexagons and tetragons (five hits), where the bromides are located simultaneously at two opposite vertices of hexagons and tetragons (see Scheme 1, top). Moreover two structures (EXUCAB and EXUCEB) present an arrangement of water molecules and bromide ions similar to the observed in compound **1**; however, only one water molecule instead of two connects the $Br_2(H_2O)_2$ tetragons. One structure presents a more complicated distribution (GOJRUT) connecting the $Br_2(H_2O)_2$ tetragons. In Figure S5 of the Supporting Information, we represent the X-ray structures of three selected

Scheme 1. Infinite Water–bromide Tapes Observed in X-ray Structures Retrieved from the CSD.[a]

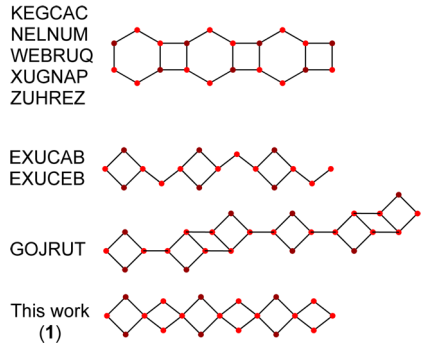

[a]The red dots represent water molecules and the brown dots represent bromide anions. For clarity, the hydrogen atoms have been omitted.

dx.doi.org/10.1021/cg401615r | Cryst. Growth Des. 2014, 14, 747–755

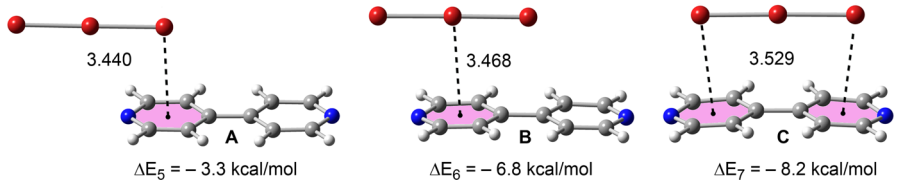

Figure 7. Optimized geometries and interaction energies of the Br_3^--bipyridine complexes at the BP86-D3/def2-TZVPD level of theory. Distances in Ångströms.

compounds to illustrate the different bromide−water geometric arrangements discussed above. It should be emphasized that the network observed in compound **1** is unprecedented in the CSD.

We have expanded our study to the noncovalent interactions observed in compound **2**, where the presence of both Br^- and Br_3^- counterions leads to the establishment of different hydrogen bonds and anion−π interactions. Moreover, π−π stacking interactions between $PTPH_3$ moieties also play a key role in the final solid state architecture, as also observed in compound **1**. As a preliminary analysis, we have studied the possible binding modes of the linear Br_3^- anion to form anion−π complexes. We have optimized at the BP86-D3/def2-TZVPD level of theory of three different complexes using a bipyridine as a theoretical model. We have used three different starting points for the optimizations, where the Br_3^- anion is located over the bipyridine ring at different positions. The optimized geometries of the complexes are shown in Figure 7, and they present significant energetic and geometric differences. The most favorable interaction energy obtained when the three bromide atoms are located over the bipyridine molecule, $\Delta E_7 = -8.2$ kcal/mol (denoted as C, see Figure 7, right), followed by the complex where the central bromine atom of the Br_3^- anion is located over one pyridine π-system (B), $\Delta E_5 = -6.8$ kcal/mol. Finally, the complex with only a single bromine atom located over the bipyridine molecule (A) is the least favorable one ($\Delta E_4 = -3.3$ kcal/mol). It should be emphasized that these preliminary results for Br_3^- anion can also be used as a model for understanding the behavior of the much more common triiodide anion, which is currently under investigation in our group.

The presence of the Br_3^- anion in the solid state of compound **2** allows us to verify the aforementioned preliminary results. In Figure 8, we show a fragment of the X-ray structure where two Br_3^- ions are located at opposite faces of the $PTPH_3$ cation. The interaction labeled as anion−π_1, corresponds to the C binding mode computed for the model system that is the most favorable orientation. At the opposite side, the interaction labeled as anion−π_2 corresponds to the B complex, which is also a favorable orientation. These results suggest that the anion−π interactions are important in governing the crystal packing of compound **2**. Additionally, the experimental anion−π distances are in good agreement with the values obtained from the theoretical DFT study (see Figures 7 and 8).

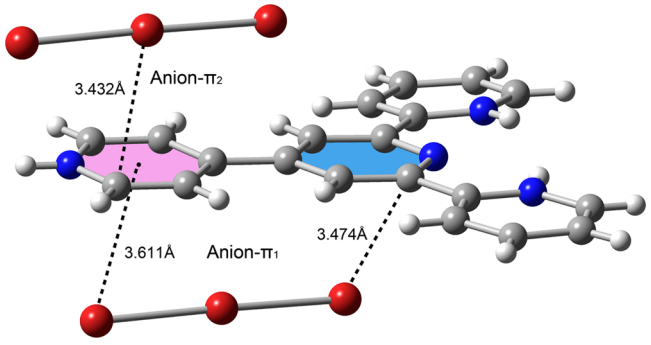

Figure 8. Anion−π interactions observed in the X-ray structure of compound **2**.

Finally, we have used the Bader's theory of "atoms in molecules", which provides an unambiguous definition of chemical bonding, to further describe the noncovalent interactions presented above. The AIM theory has been successfully used to characterize and understand a great variety of interactions; therefore, it is adequate to analyze the new interactions described above. In Figure 9, we show the AIM analysis of the anion−π/π−π/π−anion assembly of compound **1** and the inverse sandwich anion−π−anion in compound **2**. As can be observed for compound **1**, each anion−π interaction is characterized by the presence of one bond critical point that connects the bromide atoms with either one carbon or one nitrogen atom of the $PTPH_3$ cation. The π−π stacking interaction is characterized by the presence of two bond critical points (red spheres) that connect the two pyridine moieties. The stacking interaction is further characterized by the presence of three ring critical points (yellow spheres) and two cage critical points (green spheres). In compound **2**, both anion−π interactions are characterized by the presence of several bond critical points that connect the bromine atoms of the Br_3^- anions with several carbon atoms of the $PTPH_3$ cation. The Br_3^- anion that adopt the most favorable C orientation is connected to $PTPH_3$ by four bond critical points and, consequently, three ring critical points are also generated. The other Br_3^- anion that adopts the B orientation is only connected to $PTPH_3$ by three bond critical points and two ring critical points, in agreement with the energetic result. The value of the Laplacian of the charge density computed at the bond critical points in both complexes is positive, as is common in closed-shell interactions.

CONCLUSIONS

Two new pH dependent $PTPH_3$ complexes show different structural architectures conforming the versatility of the PTP ligand in combination to bromide anions. The solid state structure shows that the participation of the pyridine ring in hydrogen-bonding interactions reinforces the concurrent anion−π interaction. In both the compounds, the anions are in close proximity to the electron-deficient PTP cores, forming distinctive anion−π interactions. This work demonstrates that the anions have the ability to link cationic moiety together via anion−π interactions and provides useful supramolecular anion−π/π−anion and anion−π/π−π/π−anion type network for self-assembly progression. The experimental investigation of the role of anion−π interactions in solid state chemistry gives credence to the role of anion−π interactions as a valuable

dx.doi.org/10.1021/cg401615r | Cryst. Growth Des. 2014, 14, 747−755

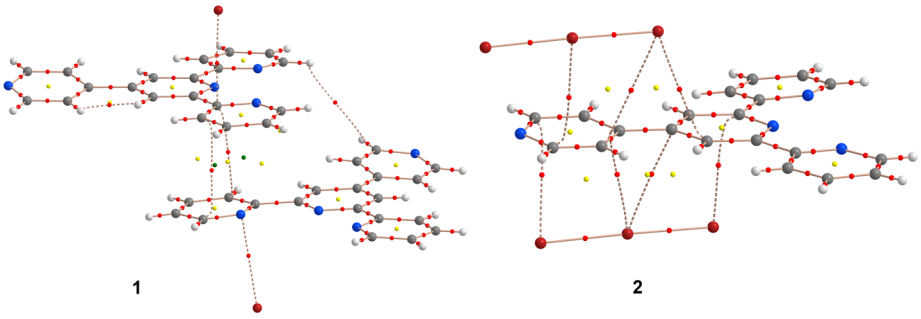

Figure 9. AIM analysis of compounds **1** and **2**. Bond, ring, and cage critical points are represented by red, yellow and green spheres, respectively. The bond paths connecting bond critical points are also represented by dashed lines.

supramolecular interaction in building multidimentional structures. In addition, the computational study has been extended to both complexes, highlighting the impact of the anion−π interaction on the final self-assembly structure. Anion−π interactions, in concert with π−π stacking and hydrogen-bonding interactions are crucial for the crystal packing phenomena of both the compounds. In compound **1**, the presence of a water−bromide cluster is also remarkable, where a mutual reinforcement of the two types of hydrogen-bonding interactions has been demonstrated computationally.

■ ASSOCIATED CONTENT

Supporting Information

X-ray crystallographic data in CIF format for **1** and **2** (CCDC nos. 963657 and 963658 for **1** and **2**, respectively). XRPD patterns of **1** and **2** and PTP ligand (Figure S1), crystal data and structure refinement parameters for **1** and **2** (Table S1), and Figures S2−S5. This material is available free of charge via the Internet at http://pubs.acs.org.

■ AUTHOR INFORMATION

Corresponding Authors

*E-mail: toni.frontera@uib.es.

*E-mail: smukhopadhyay@chemistry.jdvu.ac.in.

Notes

The authors declare no competing financial interest.

■ ACKNOWLEDGMENTS

P. M. thanks Council of Scientific and Industrial Research (New Delhi, India) for a Senior Research Fellowship [09/096(0641)2010-EMR-I]. M.M. gratefully acknowledges the University Grants Commission (New Delhi) for a junior research fellowship. S.M. is grateful to the PURSE programme in the Department of Chemistry, Jadavpur University for partial financial support of this work. This work was supported by the DGICYT of Spain (projects CTQ2011-27512/BQU and CONSOLIDER INGENIO 2010 CSD2010-00065, FEDER funds) and the Direcció General de Recerca i Innovació del Govern Balear (project 23/2011, FEDER funds).

■ REFERENCES

(1) (a) Schneider, H. J. *Angew. Chem., Int. Ed.* **2009**, *48*, 3924−3977. (b) Lehn, J.-M. *Supramolecular Chemistry*; VCH: Weinheim, Germany, 1995. (c) Steed, J. W.; Atwood, J. L. *Supramolecular Chemistry*; Wiley: Chichester, U.K., 2000.

(2) (a) Desiraju, G. R. *Acc. Chem. Res.* **2002**, *35*, 565−573. (b) Desiraju, G. R. *Nature* **2001**, *412*, 397−400. (c) Lee, H. M.; Suh, S. B.; Lee, J. Y.; Tarakeshwar, P.; Kim, K. S. J. *Chem. Phys.* **2000**, *112*, 9759−9772. (d) Hong, B. H.; Lee, J. Y.; Lee, C.-W.; Kim, J. C.; Bae, S. C.; Kim, K. S. *J. Am. Chem. Soc.* **2001**, *123*, 10748−10749. (e) Steiner, T. *Angew. Chem., Int. Ed.* **2002**, *41*, 48−76.

(3) (a) Hunter, C. A.; Sanders, J. K. M. *J. Am. Chem. Soc.* **1990**, *112*, 5525−5534. (b) Burley, S. K.; Petsko, G. A. *Science* **1985**, *229*, 23−28. (c) Kim, K. S.; Tarakeshwar, P.; Lee, J. Y. *Chem. Rev.* **2000**, *100*, 4145−4185. (d) Das, A.; Jana, A. D.; Seth, S. K.; Dey, B.; Choudhury, S. R.; Kar, T.; Mukhopadhyay, S.; Singh, N. J.; Hwang, I.-C.; Kim, K. S. *J. Phys. Chem. B* **2010**, *114*, 4166−4170. (e) Seth, S. K.; Sarkar, D.; Kar, T. *CrystEngComm* **2011**, *13*, 4528−4535. (f) Seth, S. K.; Sarkar, D.; Jana, A. D.; Kar, T. *Cryst. Growth Des.* **2011**, *11*, 4837−4849. (g) Seth, S. K.; Manna, P.; Singh, N. J.; Mitra, M.; Jana, A. D.; Das, A.; Choudhury, S. R.; Kar, T.; Mukhopadhyay, S.; Kim, K. S. *CrystEngComm* **2013**, *15*, 1285−1288. (h) Manna, P.; Seth, S. K.; Mitra, M.; Das, A.; Singh, N. J.; Choudhury, S. R.; Kar, T.; Mukhopadhyay, S. *CrystEngComm* **2013**, *15*, 7879−7886.

(4) (a) Ma, J. C.; Dougherty, D. A. *Chem. Rev.* **1997**, *97*, 1303−1324. (b) Kim, K. S.; Lee, J. Y.; Lee, S. J.; Ha, T.-K.; Kim, D. H. *J. Am. Chem. Soc.* **1994**, *116*, 7399−7400.

(5) (a) Nishio, M.; Hirota, M.; Umezawa, Y. In *The C−H/π Interaction: Evidence, Nature, Consequences*; Wiley-VCH: New York, 1998. (b) Nishio, M. *CrystEngComm* **2004**, *6*, 130−156. (c) Seth, S. K.; Sarkar, D.; Roy, A.; Kar, T. *CrystEngComm* **2011**, *13*, 6728−6741.

(6) (a) Egli, M.; Sarkhel, S. *Acc. Chem. Res.* **2007**, *40*, 197−205. (b) Mooibroek, T. J.; Gamez, P.; Reedijk, J. *CrystEngComm* **2008**, *10*, 1501−1515. (c) Ran, J.; Hobza, P. *J. Chem. Theory Comput.* **2009**, *5*, 1180−1185. (d) Barceló-Oliver, M.; Estarellas, C.; García-Raso, A.; Terrón, A.; Frontera, A.; Quinonero, D.; Molins, E.; Deyá, P. M. *CrystEngComm* **2010**, *12*, 362−365. (e) Estarellas, C.; Frontera, A.; Quinonero, D.; Deyá, P. M. *Cent. Eur. J. Chem.* **2011**, *9*, 25−34. (f) Seth, S. K.; Saha, I.; Estarellas, C.; Frontera, A.; Kar, T.; Mukhopadhyay, S. *Cryst. Growth Des.* **2011**, *11*, 3250−3265. (g) Brooker, S.; White, N. G.; Bauzá, A.; Deyà, P. M.; Frontera, A. *Inorg. Chem.* **2012**, *51*, 10334−10340.

(7) Quinonero, D.; Garau, C.; Rotger, C.; Frontera, A.; Ballester, P.; Costa, A.; Deyá, P. M. *Angew. Chem., Int. Ed.* **2002**, *41*, 3389−3392.

(8) (a) Frontera, A.; Saczewski, F.; Gdaniec, M.; Dziemidowicz-Borys, E.; Kurland, A.; Deyá, P. M.; Quinonero, D.; Garau, C. *Chem.—Eur. J.* **2005**, *11*, 6560−6567. (b) Mascal, M. *Angew. Chem., Int. Ed.* **2006**, *45*, 2890−2893. (c) Gil-Ramirez, G.; Escudero-Adan, E. C.; Benet-Buchholz, J.; Ballester, P. *Angew. Chem., Int. Ed.* **2008**, *47*, 4114−4118. (d) Schottel, B. L.; Chifotides, H. T.; Dunbar, K. R. *Chem. Soc. Rev.* **2008**, *37*, 68−83. (e) Gamez, P.; Mooibroek, T. J.; Teat, S. J.; Reedijk, J. *Acc. Chem. Res.* **2007**, *40*, 435−444. (f) Perez-Velasco, A.; Gorteau, V.; Matile, S. *Angew. Chem., Int. Ed.* **2008**, *47*, 9603−9607. (g) Dawson, R. E.; Hennig, A.; Weimann, D. P.; Emeryl, D.; Ravikumar, V.; Montenegro, J.; Takeuchil, T.; Gabutti, S.; Mayor, M.; Mareda, J.; Schalley, C. A.; Matile, S. *Nat. Chem.* **2010**, *2*, 533−538.

(9) (a) Gorteau, V.; Bollot, G.; Mareda, J.; Perez-Velasco, A.; Matile, S. *J. Am. Chem. Soc.* **2006**, *128*, 14788−14789. (b) Gorteau, V.; Bollot, G.; Mareda, J.; Matile, S. *Org. Biomol. Chem.* **2007**, *5*, 3000−3012.

(10) Mascal, M.; Armstrong, A.; Bartberger, M. D. *J. Am. Chem. Soc.* **2002**, *124*, 6274−6276.

(11) (a) Schottel, B. L.; Chifotides, H. T.; Dunbar, K. R. *Chem. Soc. Rev.* **2008**, *37*, 68−83. (b) Hay, B. P.; Bryantsev, V. S. *Chem. Commun.* **2008**, 2417−2428. (c) Frontera, A.; Gamez, P.; Mascal, M.; Mooibroek, T. J.; Reedijk, J. *Angew. Chem., Int. Ed.* **2011**, *50*, 9564−9583. (d) Frontera, A. *Coord. Chem. Rev.* **2013**, *257*, 1716−1727.
(12) Berryman, O. B.; Hof, F.; Hynes, M. J.; Johnson, D. W. *Chem. Commun.* **2006**, 506−508.
(13) Alkorta, I.; Rozas, I.; Elguero, J. *J. Am. Chem. Soc.* **2002**, *124*, 8593−8598.
(14) (a) Kim, D.; Lee, E. C.; Kim, K. S.; Tarakeshwar, P. *J. Phys. Chem. A* **2007**, *111*, 7980−7986. (b) Han, B.; Lu, J. J.; Kochi, J. K. *Cryst. Growth Des.* **2008**, *8*, 1327−1334. (c) Estarellas, C.; Rotger, M. C.; Capo, M.; Quinonero, D.; Frontera, A.; Costa, A.; Deyá, P. M. *Org. Lett.* **2009**, *11*, 1987−1990.
(15) Seth, S. K. *CrystEngComm* **2013**, *15*, 1772−1781.
(16) (a) Infantes, L.; Chisholm, J.; Motherwell, S. *CrystEngComm* **2003**, *5*, 480−486. (b) Huneycutt, A. J.; Saykally, R. J. *Science* **2003**, *299*, 1329−1330.
(17) (a) Mei, X.; Wolf, C. *CrystEngComm* **2006**, *8*, 377−380. (b) Oxtoby, N. S.; Blake, A. J.; Champness, N. R.; Wilson, C. *Chem.—Eur. J.* **2005**, *11*, 4643−4654. (c) Sansam, B. C. R.; Anderson, K. M.; Steed, J. W. *Cryst. Growth Des.* **2007**, *7*, 2649−2653.
(18) (a) Hoog, P. d.; Gamez, P.; Mutikainen, I.; Turpeinen, U.; Reedijk, J. *Angew. Chem., Int. Ed.* **2004**, *116*, 5939−5941. (b) Lakshminarayanan, P. S.; Suresh, E.; Ghosh, P. *Angew. Chem., Int. Ed.* **2006**, *45*, 3807−3811. (c) Fernandes, R. R.; Kirillov, A. M.; da Silva, M. F. C. G.; Ma, Z.; da Silva, J. A. L.; da Silva, J. J. R. F.; Pombeiro, A. J. L. *Cryst. Growth Des.* **2008**, *8*, 782−785. (d) Dey, B.; Choudhury, S. R.; Gamez, P.; Vargiu, A. V.; Robertazzi, A.; Chen, C.-Y.; Lee, H. M.; Jana, A. D.; Mukhopadhyay, S. *J. Phys. Chem. A* **2009**, *113*, 8626−8634.
(19) (a) Wang, J.; Hanan, G. S. *Synlett* **2005**, *8*, 1251−1254. (b) Beves, J. E.; Dunphy, E. L.; Constable, E. C.; Housecroft, C. E.; Kepert, C. J.; Neuburger, M.; Price, D. J.; Schaffner, S. *Dalton Trans.* **2008**, 386−396.
(20) *Bruker SAINT*, version 6.36a; Bruker-AXS Inc.: Madison, Wisconsin, 2002.
(21) *Bruker SMART*, version 5.625 and *SADABS*, version 2.03a; Bruker AXS Inc.: Madison, Wisconsin, 2001.
(22) Sheldrick, G. M. *Acta Crystallogr., Sect. A* **2008**, *64*, 112−122.
(23) Spek, A. L. *PLATON*, Molecular Geometry Program. *J. Appl. Crystallogr.* **2003**, *36*, 7−13.
(24) Farrugia, L. J. *J. Appl. Crystallogr.* **1999**, *32*, 837−838.
(25) Ahlrichs, R.; Bär, M.; Hacer, M.; Horn, H.; Kömel, C. *Chem. Phys. Lett.* **1989**, *162*, 165−169.
(26) Boys, S. B.; Bernardy, F. *Mol. Phys.* **1970**, *19*, 553−566.
(27) Bader, R. F. W. *Chem. Rev.* **1991**, *91*, 893−928.
(28) Keith, T. A. *AIMAll* (version 13.05.06); TK Gristmill Software: Overland Park, KS, 2013.
(29) Llinares, J. M.; Powell, D.; Bowman-James, K. *Coord. Chem. Rev.* **2003**, *240*, 57−75.
(30) Ihm, H.; Yun, S.; Kim, H. G.; Kim, J. K.; Kim, K. S. *Org. Lett.* **2002**, *4*, 2897−2900.
(31) (a) Etter, M. C. *Acc. Chem. Res.* **1990**, *23*, 120−126. (b) Bernstein, J.; Davis, R. E.; Shimoni, L.; Chang, N. L. *Angew. Chem., Int. Ed.* **1995**, *34*, 1555−1573.
(32) (a) Brooker, S.; White, N. G.; Bauza, A.; Deyá, P. M.; Frontera, A. *Inorg. Chem.* **2012**, *51*, 10334−10340. (b) Estarellas, C.; Bauza, A.; Frontera, A.; Quinonero, D.; Deyá, P. M. *Phys. Chem. Chem. Phys.* **2011**, *13*, 5696−5702. (c) Estarellas, C.; Frontera, A.; Quinonero, D.; Deyá, P. M. *Phys. Chem. Chem. Phys.* **2011**, *13*, 16698−16705. (d) Frontera, A.; Gamez, P.; Mascal, M.; Mooibroek, T. J.; Reedijk, J. *Angew. Chem., Int. Ed.* **2011**, *50*, 9564−9583. (e) Estarellas, C.; Frontera, A.; Quinonero, D.; Deyá, P. M. *Angew. Chem., Int. Ed.* **2011**, *50*, 415−418.
(33) Bondi, A. *J. Phys. Chem.* **1964**, *68*, 441−451.
(34) Barceló-Oliver, M.; Baquero, B. A.; Bauzá, A.; García-Raso, A.; Terrón, A.; Mata, I.; Molins, E.; Frontera, A. *CrystEngComm* **2012**, *14*, 5777−5784.
(35) Allen, F. H. *Acta Crystallogr.* **2002**, *B58*, 380−388.